DESIGN AND SIMULATION ANALYSIS OF THE TUBER HARVEST SCREENING MACHINE
/
块茎收获物清选机的设计与模拟分析

Wenliang LIU[1)], Changyou WEI[1)], Feng LIU[1,*)], Caiyu JIANG[1)], Fei PENG[1)], Jiaqi WANG[1)]
[1)]Jilin Agricultural Machinery Research Institute, Changchun, 130022, China
Corresponding author's Email: 531845652@qq.com
DOI: https://doi.org/10.35633/inmateh-73-45

***Keywords**: Tuber harvest, Simulation, Experimental study, Vibration screening, Air separation, Flexible cleaning*

ABSTRACT
In this paper, a screening machine was designed to remove the impurities in the tuber harvest, which integrates the functions of vibration screening, air separation, and flexible polishing. Discrete element simulation analysis was carried out to investigate the movement of tuber harvest and soil in the machine and the effect of polishing and removing impurities, the rationality of the structure, and the size were verified. Orthogonal tests were designed and carried out, with the rate of impurity, loss, and crushing as indicators and crank speed, impeller speed, and polishing roller speed as factors. The optimum working parameters were obtained: crank speed 280.12 r/min, impeller speed 1056.27 r/min, polishing roller speed 405.02 r/min, the impurity content was 0.29%, the loss rate was 1.01%, and the breakage rate was 0.11%. Through experimental verification, the actual value and theoretical value are basically the same, which verifies the rationality.

摘要
本文以清除块茎收获物中掺杂的杂质为目标，设计了一种集振动筛分、风选除杂、柔性清理功能于一体的清选机；并对清选作业过程进行离散元仿真分析，探究了块茎收获物和土壤在装置内的运动情况和清选除杂作业效果，验证了装置结构和尺寸设计的合理性；设计并开展正交试验，以含杂率、损失率、破碎率为指标，曲柄转速、叶轮转速、清理辊转速为因素，通过建立二次多项式回归方程和响应面模型，预测样机的最优工作参数组合：曲柄转速 280.12 r/min、叶轮转速 1056.27 r/min、抛光辊转速 405.02 r/min，此时含杂率 0.29%、损失率 1.01%、破碎率 0.11%。对预测结果优化后进行试验验证，得到预测值和优化值相近，验证了优化参数的合理性。

INTRODUCTION
Tubers are located beneath the earth's surface, making them susceptible to soil and other impurities during harvest. Additionally, newly harvested tubers have a higher water content and are prone to mildew deterioration *(Zhou et al., 2023)*. Therefore, it is essential to promptly clean the tubers after harvest in preparation for drying, dehydration, or further processing *(Zhu et al., 2022)*.

A soil-wash cleaning system for small-sized root crops, developed by *Zhang et al. (2022)* from Henan Agricultural University, breaks and separates larger soil clods by the collision and friction between tubers, and then separates the fine impurities on the tuber surface by the friction between the tuber and the sand. This design uses sand as a detergent, which requires inputting sand first and then filtering out the sand, increasing the machine's complexity, large size, and high energy consumption. Chen *et al (2015)* and others used a flexible roller beating mechanism and a flexible rolling removing impurities mechanism and used spring teeth and flexible hammers to hit the material to complete the removing impurities operation, thereby realizing the root and soil separation of deep-rooted and stem-type medicinal materials. Due to the machine's poor operating stability, it is not suitable for operations with a large amount of feeding materials and has a high damage rate. Therefore, the existing root and soil separation technology and equipment for rhizomes cannot meet the requirements of beans and soil separation. It is necessary to conduct in-depth research on the mechanism of bean and soil separation and innovate in the structural design of the separation device. In this paper, a tuber harvest screening machine was designed to clean and remove impurities in the fluidization process, and the performance test of related operation parameters was carried out for the reference of relevant researchers.

Wenliang Liu, Associate Researcher; Changyou Wei, Research Intern; Feng Liu, Senior Engineer; Caiyu Jiang, Associate Researcher; Fei Peng, Engineer; Jiaqi Wang, Engineer.

Impurities in the harvested tubers: one is soil and grass stems mixed in the tuber harvest, and the other is soil and roots attached to the tuber skin. According to the types and characteristics of impurities in the harvest, the design scheme of the whole machine is determined. Firstly, the soil doped in the harvest is cleaned by the screening device; secondly, the grass stems are cleaned by the air separation unit; finally, the soil and roots attached to the tuber surface are cleaned by the polishing device. As shown in the design scheme in Fig. 1, the tuber harvest screening machine is mainly composed of three parts: vibrating screen motion, negative pressure air separation unit, and drum cleaning device, and each part is powered by an independent motor. The research content is very meaningful for the development of the tuber harvest screening machine technology.

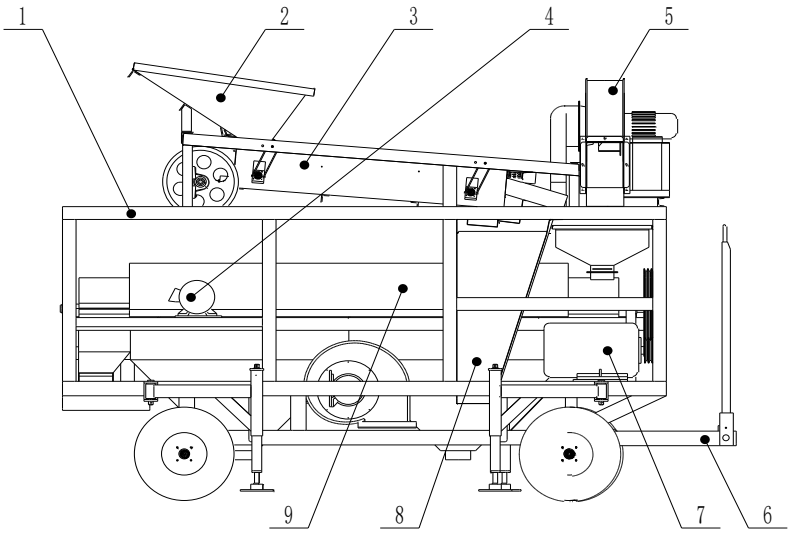

Fig. 1 - Overall structure of the tuber harvest screening machine

1 - Frame; 2 - Feeding hopper; 3 - Screening device; 4 - Screening device dynamo; 5 - Air separation unit; 6 - Hitch frame; 7 - Polishing device dynamo; 8 - Impurity removal slide; 9 - Polishing device

MATERIALS AND METHODS

Design screening device

As shown in Fig. 2, the structure of the screening device is mainly composed of pulley I, crank, connecting rod, suspension rod, and vibrating screen. The crank is firmly connected with the connecting rod, and the connecting rod is rotated with the vibrating screen. The vibrating screen is hinged with the frame by four suspension rods of equal length, and the whole vibrating screen is inclined to a certain Angle with the horizontal direction. When working, the dynamo of the screening device drives pulley I. Due to the driving connecting rod driving the vibrating screen, it makes a reciprocating swing. The amplitude can be changed by adjusting the length of the connecting rod, the vibration frequency can be changed by adjusting the crank speed, and the screen angle can be changed by adjusting the length of the suspension rods. The working principle of the screening device is to separate impurities from the tubers using a sieve based on the difference in the three-axis size of the harvested material (*Tao et al., 2023*).

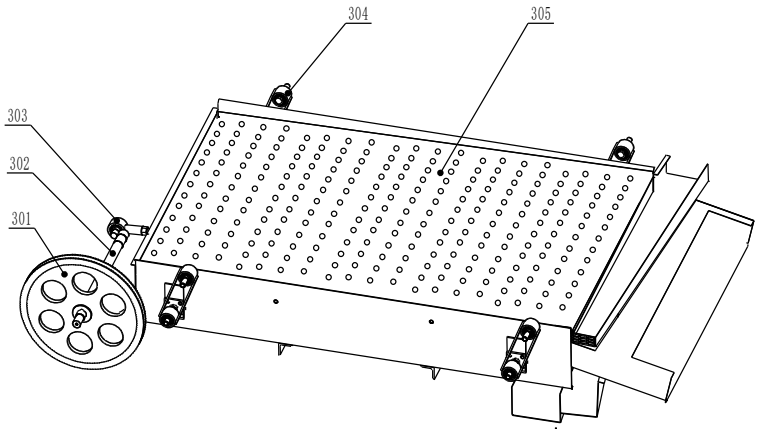

Fig. 2 - Screening device

301 - Pulley I; 302 - Crank; 303 - Connecting rod; 304 - Suspension rod; 305 - Vibrating screen

(1) Dimensional design of connecting rod and suspension rod

According to the requirements of the Agricultural Machinery Design Manual, the length of the connecting rod should be more than 5 times that of the crank, and the angle between the connecting rod and the suspension rod should be as close as possible to 90 degrees. Therefore, the length of the suspension rod should also be much larger than the length of the crank (*Chinese Academy of Agricultural Mechanization Sciences, 2007*). The length of the screening device crank is generally 23 - 30 mm, so the length of the connecting rod is designed to be 175 mm, and the length of the suspension rod is designed to be 155 mm, which is the design requirement of agricultural machinery.

(2) Design vibration direction angle and screen surface inclination angle

Directly, the vibration direction angle ε and the screen surface inclination angle α affect the motion speed of the material and the dispersion on the screen surface. Relevant studies have shown that $\varepsilon+\alpha$ is usually 5° - 15°, the larger the $\varepsilon+\alpha$, the larger the amplitude of the screening device and the stronger the separation capacity *(Du et al., 2022; Qiu et al., 2022)*. Combined with the screen surface load and separation effect, the design takes $\varepsilon+\alpha=11°$, $\alpha=5°$, $\varepsilon=6°$.

(3) Measuring friction angle

Using the inclined plane method, after many tests, the average result is obtained as the friction angle φ: friction angle $\varphi=28°$.

(4) Analyzing vibration status and calculating crank speed

To get a better screening effect, the tubers should try to keep in contact with the screen surface at all times and not be thrown up when on the screen. At the same time, the forward sliding distance of tubers on the screen surface should be greater than the reverse sliding distance to achieve the feeding function *(Tong et al., 2020; Ishtiaque et al., 2022; An et al., 2022)*. According to this operation requirement, it is necessary to analyze the vibration state of the tuber on the screen. As shown in Fig. 3, it is assumed that the vibrating screen moves in the direction of OM in a positive direction, while the crank rotates in a clockwise direction.

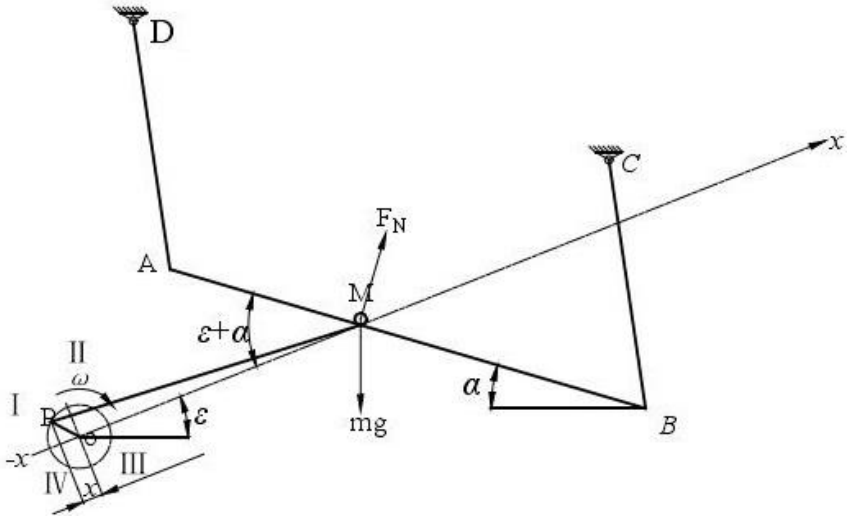

Fig. 3 - Sketch of vibrating screen motion

The vibrating screen motion can be expressed as follows:

$$\text{Displacement: } x=-r\cos\omega t \quad (1)$$

$$\text{Linear velocity: } v=x'=\frac{d_x}{d_t}=\omega r\sin\omega t \quad (2)$$

$$\text{Acceleration: } a=x''=\frac{d^2x}{dt^2}=\omega^2 r\cos\omega t \quad (3)$$

where: x - displacement, m; r - crank length, m; ω - angular velocity, rad/s; v - linear velocity, m/s; a - acceleration, m/s^2; t - time, s.

As shown in Fig. 3, according to formula (3), the acceleration is positive and the direction is to the right, when the crank OP is located in the I and IV quadrants. The tuber moves with the shaker and the acceleration is consistent with the shaker acceleration. The inertia force I of the tuber on the screen is to the left, and the formula is $I=-ma=-m\omega^2 r\cos\omega t$. where: I - inertial force, N; m- mass, kg; a - acceleration, m/s^2. At this time, the forces acting on the tuber are inertia force I, gravity mg, support reaction force F_N, friction force f,

where: in friction force $f = \mu F_N = F_N \tan\varphi$.

So, the screen surface support reaction:

$$F_N = mg\cos\alpha - I\sin(\varepsilon+\alpha)$$

Set a_s as the acceleration of tuber sliding upward along vibrating screen, then:

$$ma_s = -I\cos(\varepsilon+\alpha) - mg\sin\alpha - f \quad (4)$$

Substituting I. f into the above formula is:

$$ma_s = m\omega^2 r\cos\omega t\cos(\varepsilon+\alpha) - mg\sin\alpha - [mg\cos\alpha + m\omega^2 r\cos\omega t\sin(\varepsilon+\alpha)]\frac{\sin\varphi}{\cos\varphi} \quad (5)$$

m is divided by both sides of the equation and then multiplied by $\cos\varphi$, so the following can be obtained:

$$\cos\varphi\, a_s = \omega^2 r\cos\omega t[\cos(\varepsilon+\alpha)\cos\varphi - \sin(\varepsilon+\alpha)\sin\varphi] - g(\sin\alpha\cos\varphi + \cos\alpha\sin\varphi)$$

$$= \omega^2 r\cos\omega t\cos(\varepsilon+\alpha+\varphi) - g\sin(\alpha+\varphi) \quad (6)$$

$\varepsilon+\alpha = 11°$ and $\varphi = 28°$ are known, then $\cos(\varepsilon+\alpha+\varphi) > 0$.

Divide $\cos(\varepsilon+\alpha+\varphi)$ by both sides of Formula (6):

$$\frac{\cos\varphi}{\cos(\varepsilon+\alpha+\varphi)}a_s = \omega^2 r\cos\omega t - g\frac{\sin(\alpha+\varphi)}{\cos(\varepsilon+\alpha+\varphi)} \quad (7)$$

From $\varphi = 28°$, it can be inferred that $\cos\varphi > 0$, and since $\cos(\varepsilon+\alpha+\varphi)>0$, $\frac{\cos\varphi}{\cos(\varepsilon+\alpha+\varphi)}>0$, according to Formula (7), when $a_s > 0$, the tuber slides upwards along the vibrating screen. At this point:

$$\omega^2 r\cos\omega t > g\frac{\sin(\alpha+\varphi)}{\cos(\varepsilon+\alpha+\varphi)} \quad (8)$$

Similarly, the condition for the tuber to slide downwards along the screen surface is:

$$-\omega^2 r\cos\omega t > g\frac{\sin(\alpha-\varphi)}{\cos(\varepsilon+\alpha-\varphi)} \quad (9)$$

The tubers are thrown on the screen under the following conditions:

$$-\omega^2 r\cos\omega t \geq g\frac{\cos\alpha}{\sin(\varepsilon+\alpha)} \quad (10)$$

$k_s = g\frac{\sin(\alpha+\varphi)}{\cos(\varepsilon+\alpha+\varphi)}$, is called the up slip index. $k_x = g\frac{\sin(\alpha-\varphi)}{\cos(\varepsilon+\alpha-\varphi)}$, is called the down slide index (*Fu, 2019*). $k_p = g\frac{\cos\alpha}{\sin(\varepsilon+\alpha)}$, is called the throwing index. Given $\varepsilon = 6°$, $\alpha = 5°$, $\varphi = 28°$, the calculation can be: $k_s = 6.87$; $k_x = 4$; $k_p = 51.16$.

According to Formulas (8) and (10), when $\cos\omega t = 1$, $-\cos\omega t = 1$, the crank critical angular velocity formula can be obtained:

$$\omega_s = \sqrt{\frac{k_s}{r}} \quad (11)$$

$$\omega_p = \sqrt{\frac{k_p}{r}} \quad (12)$$

And since $n = \frac{30\omega}{\pi}$, Formulas (11) and (12) can be transformed into:

$$n_s = \frac{30}{\pi}\sqrt{\frac{k_s}{r}} \quad (13)$$

$$n_p = \frac{30}{\pi}\sqrt{\frac{k_p}{r}} \quad (14)$$

where n_s represents the crank speed when sliding up, r/min; n_p represents the crank speed when thrown up, r/min; r represents the length of the crank, m; ks represents the up slide index; kp represents the upthrow index.

In order that the forward sliding distance of the tuber on the screen surface should be larger than the reverse sliding distance, the crank speed n should be: $n_s < n < n_p$.

Substituting the minimum crank length $r_{min} = 23$ mm, $k_s = 6.87$, $k_p = 51.16$ into Formula (13) and (14), it can be obtained $n_s = 165.12$ r/min, $n_p = 450.6$ r/min, and the obtained crank speed range of screening device 165.12 r/min - 450.6 r/min.

Design Air separation unit

As shown in Fig. 4, the air separation unit consists of a support, a driving motor, and a fan casting. The grass roots separated and mixed in the tubers are discharged from the machine and wind power is generated by fan rotation, which is the working principle of the Air separation unit *(Zhou et al., 2022; Zhao et al., 2023).* The Air separation unit is installed above the end of the vibrating screen, the suction outlet is toward the screen surface, and the outlet is toward the outside of the body. The driving motor is a centrifugal fan with a power of 2.2 kW and a rated speed of 2900 r/min.

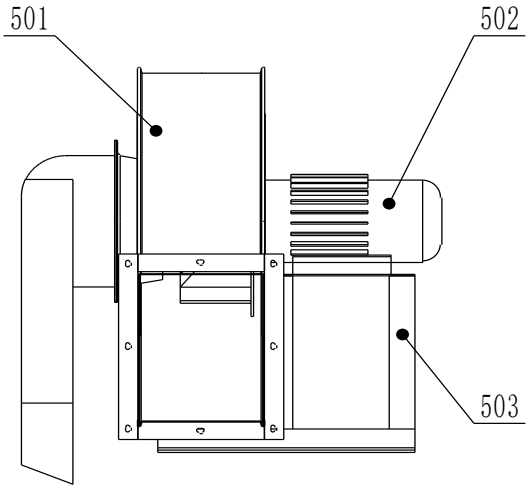

Fig. 4 - Air separation unit
501 - Fan casting; 502 - Air separation unit dynamo; 503 - Support

Design polishing device

The structure of the polishing device is shown in Fig. 5, which is mainly composed of a polishing room, a feed hopper, a pulley II, a settling box, an impurity removal fan, and an outlet hopper. The polishing room is of horizontal structure. The polishing roller, as shown in Fig. 6, consists of a polishing shaft and a nylon brush mounted on it *(Wang et al., 2018; Zhang et al., 2023)*. At work, the tubers enter the cleaning room from the hopper, and as the polishing roller rotates along the spiral to the discharge port, the tubers rub against each other in the fluidized movement process. At the same time, the nylon brush frictions the surface of the tubers. Under the action of multiple forces, the tubers are separated from the surface attachments such as soil and roots, and discharged through the hopper, and the soil impurities are discharged through the lower shell through the settling box. The impurities of the root are blown out of the machine under the action of the impurity fan.

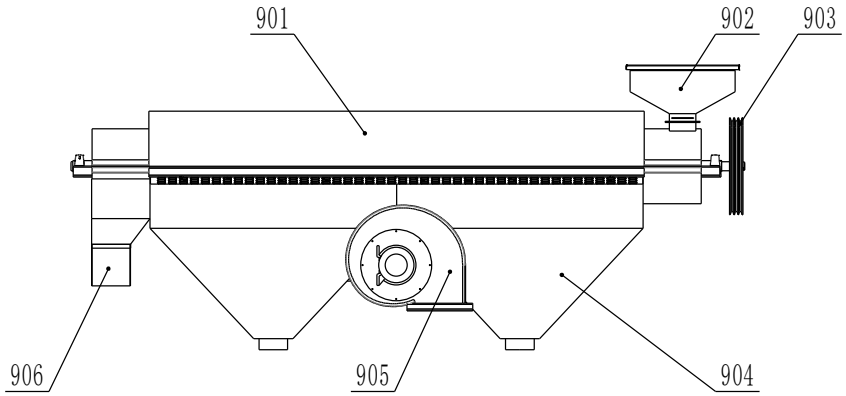

Fig. 5 - Polishing device
901- Polishing room; 902 - Feed hopper; 903 - Pulley II; 904 - Settling box; 905 - Impurity removal fan; 906 - Outlet hopper

90031 - Nylon brush; 90032 - Polishing shaft
Fig. 6 - Polishing roller

Calculate the polishing roller diameter

According to the Agricultural Machinery Design Manual, the calculation formula for the design parameters of the polishing roller (including the brush installed on the roller shaft) is:

$$A_q = \frac{60\pi n e D^2}{Q} \quad (15)$$

$$l = e D \quad (16)$$

where: A_q - movement area per unit output of the polishing roller, 70 m²/kg; n - polishing roller speed, 400r/min; e- polishing roller length and diameter ratio, 8; polishing roller diameter, m; and Q - polishing machine output per hour, 1000 kg/h.

According to Formula (15), the diameter of the cleaning roller D = 0.34 m = 340 mm can be obtained, and according to Formula (16), the length of the cleaning roller l = 2720 mm.

Calculate the polishing roller speed

The speed of the polishing roller determines the movement speed and collision force of the crop. The calculation formula for the speed of the cleaning roller is:

$$n = \frac{60v}{\pi D} \quad (17)$$

where n - cleaning roller speed, r/min; v - cleaning roller linear speed, m/s; and D - diameter of the cleaning roller, m.

Generally, the linear speed of the cleaning roller is 6 m/s - 10 m/s (*Yang et al., 2023; Ji et al., 2021*). According to Formula (17), the speed of the cleaning roller is 337 r/min - 562 r/min.

Discrete element simulation analysis

It is difficult to observe the operation process because the entire device is a closed structure. Discrete element simulation analysis is carried out by EDEM software to observe the movement and the operating effect of tubers and soil and fibrous roots in the device, and verify the rationality of the parameter and structural design.

(1) Establishing models for crops, soil, and fibrous roots

In this paper, the length of the tuber modeling is 7 mm; the width is 13 - 14 mm, the height is 12 - 13 mm and the soil diameter is 3 mm. The length of the root is 5 mm. The bonding bond between the tuber, soil and fibrous roots can withstand the force and deformation caused by collision, friction, extrusion, kneading, etc. When it reaches a certain degree, the bonding fails and the soil or fibrous root particles are separated from the parent (*Jiang et al., 2023; Yu, 2022*). As shown in Fig. 7, the model is established through particle combination, including the tuber, soil, and bonding models.

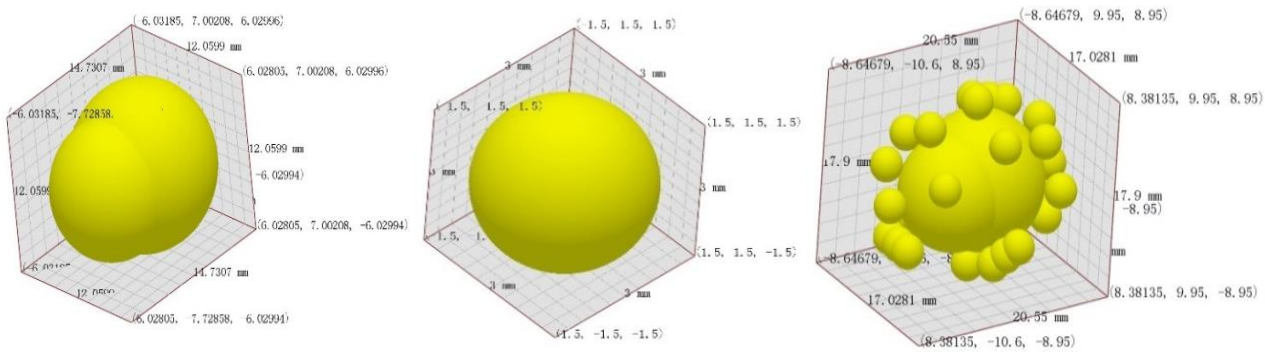

a - tuber model *b - soil particle model* *c- Crop bonding model*

Fig. 7 - Model building

(2) Simulation process

During the simulation, the particle factory is set up and the particles are generated dynamically inside the hopper. The particles entering the polishing chamber through the hopper are polished for simulation and discharged from the rear discharge port after the whole polishing process (*Zhang et al., 2022; Sadek et al., 2021; Sarkar et al., 2021*).

The particle generation speed is set as 1500 grains/s and the line speed into the hopper is set as 0.7 m/s. The acceleration of gravity is 9.8 m/s². Set the fixed time step to the time step of 16.04%, the step size to 2E - 5 s, and the mesh size to 2.5 R. The simulation situation is shown in Fig. 8.

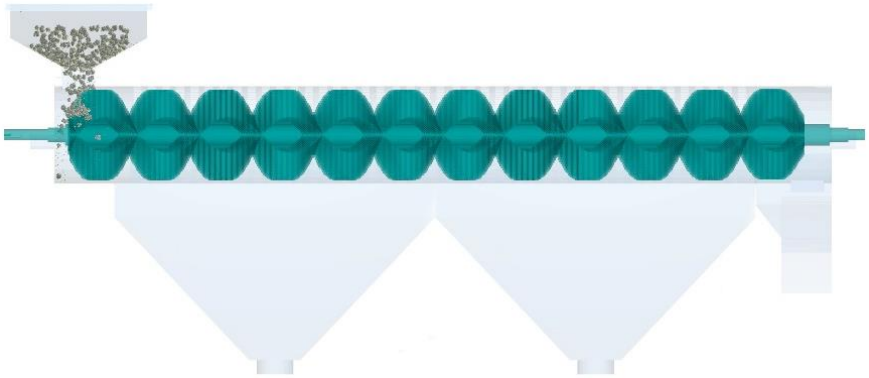

（a）- t=1s

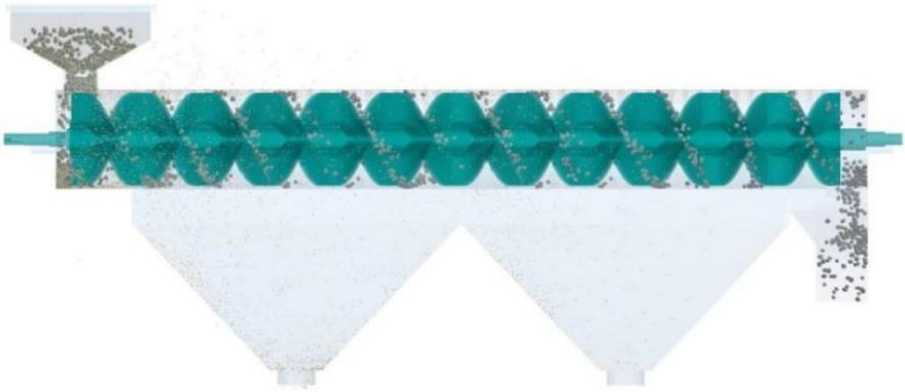

（b）t=7s

Fig. 8 - Simulation situation

(3) Analyze simulation results

From the simulation process, it can be clearly seen that the effect of the crop polishing operation throws off more impurities in the beginning stage. At the end of the polishing chamber, there were basically no impurities falling, indicating that the length of the polishing roller is reasonable. And because there were more crops gathered under the polishing room near the settling box, the polishing effect was best here. However, in the actual operation process, the entire polishing room would be filled with crops, and this effect would be achieved everywhere in the polishing room.

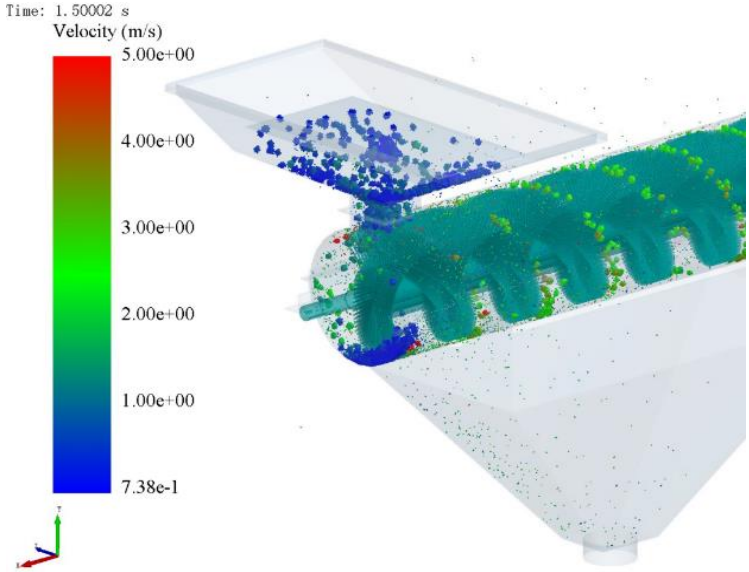

Fig. 9 - Article velocity vector diagram of simulation process

The particles' velocity field distribution in the simulation process is shown in Fig. 9. It can be seen that the crops enter the polishing room through the hopper and contact the polishing roller at the front of the polishing room. Due to the impact of the rotating polishing roller, the speed is relatively fast.

The particles close to the nylon brush are thrown up by the nylon brush rotation, and a certain acceleration is obtained, and the speed is also relatively fast. The particles between the spiral nylon brush are forced to withstand the thrust action, rotate axially, and move toward the discharge port at a uniform speed.

RESULTS

Design factor level

The impurity rate, loss rate, and crushing rate selected during the experiment were used as evaluation indicators, and the feeding amount remained constant at 1000 kg/h.

(1) The impurity rate is calculated as follows:

$$\eta_1 = \frac{n_1}{n_2} \quad (18)$$

Where η_1 represents the impurity content, %; n_1 represents the mass of impurities in the material after operation, kg; and n_2 represents the mass of mixture after operation, kg. *(Ishtiaque et al., 2022)*

(2) The loss rate is calculated as follows:

$$\eta_2 = \frac{n_3}{n_3+n_4} \quad (19)$$

Where η_2 represents the loss rate, %; n_3 represents the loss of tubers, kg; and n_4 represents the mass of tuber harvested through the device, kg.

(3) The crushing rate is as follows:

$$\eta_3 = \frac{n_5}{n_6} \quad (20)$$

$Where\ \eta_3$ represents the crushing rate, %; n_5 represents the mass of broken tubers, kg; and n_6 represents the mass of harvested tubers, kg. (*An et al., 2022; Fu, 2019; Zhou et al., 2022*)

Test design

In advance, the single-factor test was carried out to develop the rule that the three test indexes, including the impurity rate, loss rate, and crushing rate, were affected by five factors (the screen inclination angle of the screening device, the crank speed of the screening device, the impeller speed of the air separation unit, the polishing roller speed of the polishing device, and the clearance of the polishing chamber of the polishing device). It is concluded that the factors and levels that have a great influence on the cleaning, screening and impurity removal effects of tuber harvest were as follows: crank speed: 254 r/min - 314 r/min, impeller speed: 900 r/min - 1700 r/min, and polishing roller speed: 378 r/min - 452 r/min. According to the above test results, the factors and levels of the orthogonal test were selected: crank speed: 254, 284, 314 r/min, impeller speed: 900, 1100, 1300 r/min, and polishing roller speed: 380, 410, 440 r/min. The test was designed using Design-Expert software, and 17 groups of tests were estimated. The test data results are shown in Table 1.

Table1

Orthogonal test table and results

Number	Crank speed r/min	Impeller speed r/min	Polishing roller speed r/min	Impurity rate %	Loss rate %	Crushing rate %
1	284	1300	380	0.44	1.52	0.24
2	314	1100	440	0.52	1.76	0.19
3	254	900	410	0.42	1.42	0.17
4	284	1100	410	0.32	1.03	0.13
5	254	1100	440	0.47	1.53	0.16
6	284	1100	410	0.29	0.96	0.12
7	284	900	380	0.39	1.33	0.17
8	314	1300	410	0.52	1.78	0.25
9	284	1100	410	0.29	1.05	0.12
10	254	1100	380	0.44	1.42	0.14
11	284	1100	410	0.31	1.04	0.12
12	254	1300	410	0.47	1.59	0.24
13	314	900	410	0.46	1.61	0.19
14	284	1300	440	0.54	1.66	0.26
15	314	1100	380	0.43	1.63	0.17
16	284	1100	410	0.3	1.09	0.11
17	284	900	440	0.43	1.43	0.18

The regression equations containing the impurity rate, loss rate, and crushing rate are obtained by fitting the data.

$$Y_1 = 0.30 + 0.016A + 0.034B + 0.033C + 0.015AC + 0.015BC + 0.090A^2 + 0.075B^2 + 0.073C^2 \quad (21)$$

$$Y_2 = 1.03 + 0.10A + 0.095B + 0.060C + 0.010BC + 0.33A^2 + 0.23B^2 + 0.22C^2 \quad (22)$$

$$Y_3 = 0.12 + 0.011A + 0.035B + 0.023A^2 + 0.070B^2 + 0.023C^2 \quad (23)$$

where: Y_1 - impurity rate; Y_2 - loss rate; Y_3 - crushing rate; A - crank speed; B - impeller speed; C - polishing roller speed.

Interpretation of results

Analyze the significance of impurity rate

Table2

Analysis of variance of impurity rate

Source of variation	Quadratic sum	Degree of freedom	Mean square error	*F*-value	*P*-value	Significance
Model	0.11	9	0.012	63.86	＜0.0001	Significant
A	2.113E-003	1	2.113E-003	10.91	0.0131	
B	9.113E-003	1	9.113E-003	47.08	0.0002	
C	8.450E-003	1	8.450E-003	43.65	0.0003	
AB	2.500E-005	1	2.500E-005	0.13	0.7299	
AC	9.00E-004	1	9.000E-004	4.65	0.0680	
BC	9.00E-004	1	9.00E-004	4.65	0.0680	
A^2	0.034	1	0.034	177.17	＜0.0001	
B^2	0.024	1	0.024	123.17	＜0.0001	
C^2	0.022	1	0.022	115.12	＜0.0001	
Residuals	1.355E-003	7	1.936E-004			
Undrafted item	6.750E-004	3	2.250E-004	1.32	0.3837	Not significant
Pure error	6.800E-004	4	1.700E-004			
Sum total	0.11	16				

According to the data in Table 2, P-value 0.0001 < 0.01, F-value = 63.86, the model effect was significant, and the P - value of the missing item was 0.3837 > 0.05, indicating that there was no missing factor and the model was stable. R^2 = 0.988, regression items A^2, B^2 and C^2 were extremely significant under P < 0.001, regression items A, B and C were significant under P < 0.05, and the remaining items P > 0.1 were not significant. The factors that affected the impurity content were A > B > C, that is, crank speed > impeller speed > polishing roller speed.

Analyze the significance of loss rate

Table3

Analysis of variance of loss rate

Source of variation	Quadratic sum	Degree of freedom	Mean square error	*F*-value	*P*-value	significance
Model	1.18	9	0.13	90.32	＜0.0001	significant
A	0.084	1	0.084	57.85	0.0001	
B	0.072	1	0.072	49.70	0.0002	
C	0.029	1	0.029	19.82	0.003	
AB	0.000	1	0.000	0.000	1.0000	
AC	1.000E-004	1	1.000E-004	0.069	0.8006	
BC	4.000E-004	1	4.000E-004	0.28	0.6160	
A^2	0.47	1	0.47	321.37	＜0.0001	
B^2	0.23	1	0.23	157.33	＜0.0001	
C^2	0.20	1	0.20	137.73	＜0.0001	
Residuals	0.010	7	1.453E-003			
Undrafted item	1.250E-003	3	4.167E-004	0.19	0.9002	not significant
Pure error	8.920E-003	4	2.230E-003			
Sum total	1.19	16				

From the data in Table 3, P < 0.0001, F = 90.32, the model was significant, and P = 0.9002 > 0.05 of the missing item indicates that was no missing factor and the model was stable. R^2 = 0.9915. When P < 0.001, regression items A^2, B^2 and C^2 were extremely significant; when P < 0.05, regression items A, B and C were significant, while the other items were not. The factors affecting the loss rate are as follows: A > B > C; namely, crank speed > impeller speed > polishing roller speed.

Analyze the significance of crushing rate

Table4

Analysis of variance of crushing rate

Source of variation	Quadratic sum	Degree of freedom	Mean square error	*F*-value	*P*-value	Significance
Model	0.038	9	4.249E-003	79.31	＜0.0001	Significant
A	1.012E-003	1	1.012E-003	18.90	0.0034	
B	9.800E-003	1	9.800E-003	182.93	＜0.0001	
C	6.125E-004	1	6.125E-004	11.43	0.0117	
AB	2.500E-005	1	2.500E-005	0.47	0.5165	
AC	0.000	1	0.000	0.000	1.0000	
BC	2.500E-005	1	2.500E-005	0.47	0.5165	
A^2	2.132E-003	1	2.132E-003	39.73	0.0002	
B^2	0.021		0.021	385.12	＜0.0001	
C^2	2.132E-003	1	2.132E-003	39.79	0.0004	
Residuals	3.750E-004	7	5.357E-005			
Undrafted item	1.750E-004	3	5.833E-005	1.17	0.4262	not significant
Pure error	2.000E-004	4	5.000E-005			
Sum total	0.039	16				

Table 4 shows that the regression model with P < 0.0001 was extremely significant. The missing item (P = 0.4262 > 0.05) was not significant, indicating there was a good fit. By analyzing the P-values of the primary and secondary and interaction terms of each factor, it can be seen that the P-values of B and B^2 were < 0.0001, and the influence was extremely significant; the P-values of A, C, A^2 and C^2 were < 0.05, and the influence was significant. According to the F-value in the table, the main order of factors was B > A > C, that is, impeller speed > crank speed > polishing roller speed.

Parameter optimization and experimental verification

The three selected factors were optimized by Design-Expert 8.0.6 software to predict the test indexes and obtain the optimal parameter combination of optimization results. In the optimization process, the three test indexes including impurity rate, loss rate and crushing rate were set to the minimum, and the optimization process and results are shown in Table 5.

Table 5

Optimization process and results

		Lower	Upper	Lower	Upper			
Name	Goal	Limit	Limit	Weight	Weight	Importance		
A:Vibrating screen crank speed	Within the range	254	314	1	1	3		
B: Fan impeller speed	Within the range	900	1300	1	1	3		
C: Polishing roller speed	Within the range	380	440	1	1	3		
Impurity rate	Minimal	0.29	0.54	1	1	5		
loss rate	Minimal	0.96	1.78	1	1	4		
Crushing rate	Minimal	0.11	0.26	1	1	3		
Solutions								
Number	**Vibrating screen crank speed**	**Fan impeller speed**	**Polishing roller speed**	**Impurity rate**	**Loss rate**	**Crushing rate**	**Desirability**	
1	280.12	1056.27	405.02	0.295172	1.0132	0.113804	0.963	Selected

The predicted results are: the crank speed was 280.12 r/min, the impeller speed was 1,056.27 r/min, and the cleaning roller speed was 405.02 r/min. The impurity rate, loss rate and crushing rate were 0.29%, 1.01%, and 0.11%, respectively.

According to the actual operating conditions and operational feasibility, the predicted results were verified. The test parameters were set as integers; the crank speed was 284 r/min, the impeller speed was 1100 r/min, and the polishing roller speed was 410 r/min. The test was repeated three times. As shown in Table 6, the average value of impurity rate, loss rate and crushing rate was basically the same as the predicted value, meeting the design requirements of the machine tools.

Table 6

Validation test results

Number of trials	Impurity rate %	Loss rate %	Crushing rate %
1	0.29	1.03	0.15
2	0.30	1.05	0.13
3	0.31	1.07	0.12
Mean	0.30	1.05	0.13

CONCLUSIONS

(1) In this paper, a kind of tuber harvest polishing machine is designed, and the screening device, air separation unit and polishing device are designed in detail and their parameters are calculated. The centrifugal volute suction fan with a power of 2.2 kW is selected for the air separation unit. The polishing device is designed as a combination structure of a double helix nylon brush and cylinder screen.

(2) The particle model of soil and fibrous roots attached to the surface of tuber harvest was established by EDEM software. The movement of tuber harvest, soil, and roots in the plant and the effect of polishing and removing impurities were analyzed by discrete element simulation, which finally verified the rationality of the structure and size design of the plant.

(3) To verify the rationality of the optimized parameters, the quadratic polynomial regression equation and response surface were employed to establish the model by determining the influence law of the interaction between different factors on the evaluation index. Among them, the impurity rate, loss rate, and crushing rate were used as evaluation indexes, and the crank speed, impeller speed, and polishing roller speed were used as factors. According to the best working parameters predicted by the software, and combined with the actual working needs of the machine, the software prediction results were optimized and verified.

The research content of this paper has certain reference significance for the design and simulation analysis of the tuber harvest screening machine. The design tested some factors that affected the operation effect due to the limitations of the test cycle and parts processing conditions. In the future, studies can be conducted on the influence of other factors, such as the inclination angle of the roller, the brush wire material, etc.

ACKNOWLEDGEMENTS

Science and technology development plan of Jilin Province “Study on Key Equipment of Whole Mechanized Operation Mode of Farmland Ginseng” (20230202037NC).

REFERENCES

[1] An, Z., Wang, R., Liu, P., & Fan, J. (2022). Design Study of a New Type of Flat Body Cleaning Device. *Journal of Electronics and Information Science*, Vol. 7(1), pp. 99-102. http://dx.doi.org/10.23977/jeis.2022.070117

[2] Chen, X.S., Ma, X., Chen, G.R., Qi, L., Wu, T., Zeng, L.C. (2015). Research on root-soil separation device for deep-rooted Chinese medicinal materials. Mechanical Design, Vol. 32 (07), pp.65-70. DOI: 10.13841/j.cnki.jxsj.2015.07.014

[3] Chinese Academy of Agricultural Mechanization Sciences (2007). *Agricultural Machinery Design Manual* (农业机械设计手册). China Agricultural Science and Technology Press, Beijing, China. (In Chinese)

[4] Du, J., Heng, Y., Zheng, K., Luo, C., Zhu, Y., Zhang, J., & Xia, J. (2022). Investigation of the burial and mixing performance of a rotary tiller using discrete element method. *Soil and Tillage Research*, Vol. 220, pp. 105349. https://doi.org/10.1016/j.still.2022.105349

[5] Fu Y. (2019). *Study on screening device for wet peanut pods* (鲜花生荚果筛选装置试验研究). Shenyang Agricultural University. (In Chinese). DOI: 10.27327/d.cnki.gshnu.2019.000323

[6] Ishtiaque, A., Singh, S., Lobell, D., Fishman, R., & Jain, M. (2022). Prior crop season management constrains farmer adaptation to warming temperatures: evidence from the Indo-Gangetic Plains. *Science of the Total Environment*, Vol. 807, pp. 151671. https://doi.org/10.1016/j.scitotenv.2021.151671

[7] Ji, J., Sang, Y., He, Z., Jin, X., & Wang, S. (2021). Designing an intelligent monitoring system for corn seeding by machine vision and Genetic Algorithm-optimized Back Propagation algorithm under precision positioning. *PloS one*, Vol. 16(7), pp. e0254544. https://doi.org/10.1371/journal.pone.0254544

[8] Jiang, Q., Liu, Y., Zhou, X., Yang, Y., Zhang, J., Jiang, B., Mao, D., Yang, Y., & Fu, Y. (2023). Intelligent Control Knowledge-Based System for Cleaning Device of Rice–Wheat Combine Harvester. *International*

Journal of Pattern Recognition and Artificial Intelligence, Vol. 37(07), pp. 2359015. https://doi.org/10.1142/S0218001423590152

[9] Qiu, W., Ma, X., Cao, H., Huang, T., She, X., Huang, M., Wang, Z., & Liu, J. (2022). Improving wheat yield by optimizing seeding and fertilizer rates based on precipitation in the summer fallow season in drylands of the Loess Plateau. *Agricultural Water Management*, Vol. 264, pp. 107489. https://doi.org/10.1016/j.agwat.2022.107489

[10] Sadek, M. A., Chen, Y., & Zeng, Z. (2021). Draft force prediction for a high-speed disc implement using discrete element modelling. *Biosystems engineering*, Vol. 202, pp. 133-141. https://doi.org/10.1016/j.biosystemseng.2020.12.009

[11] Sarkar, P., Upadhyay, G., & Raheman, H. (2021). Active-passive and passive-passive configurations of combined tillage implements for improved tillage and tractive performance: A review. *Spanish journal of agricultural research*, Vol. 19(4), pp. e02R01-e02R01. https://doi.org/10.5424/sjar/2021194-18387

[12] Tao, J., Leng, J., Lei, X., Wan, C., Li, D., Wu, Y., Yang, Q., Wang, P., Feng, B., & Gao, J. (2023). Effects of selenium (Se) uptake on plant growth and yield in common buckwheat (*Fagopyrum esculentum Moench*). *Field Crops Research*, Vol. 302, pp. 109070. https://doi.org/10.1016/j.fcr.2023.109070

[13] Tong, J., Jiang, X. H., Wang, Y. M., Ma, Y. H., Li, J. W., & Sun, J. Y. (2020). Tillage force and disturbance characteristics of different geometric-shaped subsoilers via DEM. *Advances in Manufacturing*, Vol. 8, pp. 392-404. https://doi.org/10.1007/s40436-020-00318-x

[14] Wang, Q., Wu, W., & Zhu, H. (2018). Design and test of screw cleaning mechanism for corn (玉米螺旋式清选装置的设计与试验). *Transactions of the CSAE*, Vol. 34(20), pp. 12-19. (In Chinese). DOI:10.11975/j.issn.1002-6819.2018.20.002

[15] Yang, W., Ma, X., Ma, R., & Yang, C. (2015). Design and Experiment of Drum Type Brush Removing Soil Device (滚筒式毛刷清扫土装置的设计与试验). *Journal of Agricultural Mechanization Research*, Vol. 37(12), pp. 197-200. (In Chinese). DOI:10.3969/j.issn.1003-188X.2015.12.043

[16] Yu, C. (2022). *Analysis and Simulation Test of Rice Grain Movement Trajectory in Rice Flexible Polishing Machine* (大米柔性抛光机内米粒运动轨迹分析与仿真试验). Wuhan Polytechnic University. (In Chinese). DOI: 10.27776/d.cnki.gwhgy.2022.000370

[17] Zhang, X., Liu, X., Fan, C., Pei, Y., Wang, D., Zhou, P., Chen, X., Zhao, R., Zhou, X., Song, Q., Hou, Y., Zhang, Y., Liu, R., Lin, G. (2022). A "soil-washing" dry cleaning system for small-particle root crops (一种"以土洗土"的小粒径根茎作物干洗系统). Henan Province: [P] CN202110484627.9, 2022-11-22. (In Chinese)

[18] Zhang, C., Geng, D., Xu, H., Li, X., Ming, J., Li, D., & Wang, Q. (2023). Experimental Study on the Influence of Working Parameters of Centrifugal Fan on Airflow Field in Cleaning Room. *Agriculture*, Vol. 13(7), pp. 1368. https://doi.org/10.3390/agriculture13071368

[19] Zhang, S., Fu, J., Zhang, R., Zhang, Y., & Yuan, H. (2022). Experimental study on the mechanical properties of friction, collision and compression of tiger nut tubers. *Agriculture*, Vol. 12(1), pp. 65. https://doi.org/10.3390/agriculture12010065

[20] Zhao, G., Wu, P., Liu, F., Li, S., Zhang, J., Dang, Y., Wang, L., Wang, S., Cheng, W., Cai, T., & Fan, T. (2023). Plow layer management during the fallow season can enhance the wheat productivity and resource utilization in a semi-arid region. *Soil and Tillage Research*, Vol. 228, pp. 105633. https://doi.org/10.1016/j.still.2022.105633

[21] Zhou, J., Sun, W., & Liang, Z. (2023). Research on discrete element flexible model of Jerusalem artichoke roots and tubers during harvest period (收获期菊芋根-块茎离散元柔性模型研究). *Transactions of the CSAM*, Vol. 54(10), pp. 124-132. (In Chinese). DOI: 10.6041/j.issn.1000-1298.2023.10.011

[22] Zhou, X., WANG, Z., TIAN, L., Su, Z., & Ding, Z. (2022). Numerical Simulation and Experiment of Cleaning Performance of Combine Harvester under the Action of Conical Fan. *Engineering in Agriculture, Environment and Food*, Vol. 15(2), pp. 61-71. https://doi.org/10.37221/eaef.15.2_61

[23] Zhu, C., Chen, B., Li, J., Liu, Y., Yang, L., Wang, W., & Zhang, H. (2022). Design and Testing of the Peanut Pod Cleaning Device. *Processes*, Vol. 11(1), pp. 106. https://doi.org/10.3390/pr11010106